Poskela, Aapo; Tiihonen, Armi; Palonen, Heikki; Lund, Peter D.; Miettunen, Kati

Predictive Modeling of Dye Solar Cell Degradation

Published in:
Solar RRL

DOI:
10.1002/solr.202101004

Published: 01/06/2022

Document Version
Publisher's PDF, also known as Version of record

Solar RRL
www.solar-rrl.com

Predictive Modeling of Dye Solar Cell Degradation

Aapo Poskela, Armi Tiihonen, Heikki Palonen, Peter D. Lund, and Kati Miettunen*

Degradation of dye solar cell performance based on the early changes in electrolyte color is predicted, allowing to estimate the lifetime of the dye solar cells even before their efficiency declines. Previous predictive models commonly rely on regression analysis of the predicted parameter; thus, they are unable to capture degradation before a significant decrease in performance. Degradation tests, even when accelerated, may take thousands of hours. As such, recognizing degradation trends early can lead to rewarding cuts in the duration of solar cell development pipelines. With accurate lifetime predictions, researchers can steer materials research to reach longer lifetimes in shorter cycles. The predictive power of our model relies on color changes in the electrolyte that directly correlate with the concentration of triiodide charge carriers within it, the loss of which is the predominant degradation mechanism for most liquid-electrolyte dye solar cells. By linking the physical mechanisms inside the cell, which eventually start to degrade the performance of dye solar cells, an early prediction of the lifetime can be made even when the device performance still appears stable. It is exemplified with dye solar cells that integrating architecture-specific knowledge on degradation mechanisms has potential to improve lifetime predictions for photovoltaics.

1. Introduction

A major bottleneck for commercializing emerging photovoltaic (PV) technologies is their limited lifetime due to instability.[1–4] To improve stability, experimental aging tests are often required. Real-life outdoor tests produce the most reliable results but take years or, at later stages of development, even decades to complete. Even though most solar-cell stability research uses accelerated test protocols, such as continuous illumination or increased temperatures, individual aging tests may still take several months.[5,6] As such, long testing times severely limit the number of tests that can be carried out, which in turn slows the pace of research. Not only is this a challenge for emerging PVs, but also for silicon solar cells.[6] Given this, the ability to predict the degradation of PV devices based on early markers would be a valuable tool to guide the research into stable PVs. Early markers would facilitate scheduling future experiments, and in the case of very stable samples, lifetimes could be estimated without waiting for aging test to be completed. In commercial use, early prediction methods would also allow solar panel replacements to be planned more accurately. In addition, future revenues for solar plants could be estimated more comprehensively based on the detailed information generated about maintenance needs and panel stability based on the specific environmental conditions of the plant location.

Previous approaches to PV device lifetime prediction and modeling have varied. Some studies have used material parameters, measured before the solar cell or panel was manufactured, to estimate the expected lifetime.[7,8] In contrast, others have used earlier aging studies to determine an experimental function to model further aging tests.[9–15] While most of these studies have focused on the more established silicon solar cells, predicting emerging PV is beginning to gain attention with some interesting contributions. Temperature-dependent degradation rates have been calculated and experimentally demonstrated for both organic[16,17] and perovskite solar cells.[18,19] A general extrapolative model for emerging solar cell lifetimes was developed by Rizzo et al.[20] An earlier work on dye solar cells (DSCs) by Chalkias et al.[21] comprehensively studied the degradation of DSCs under different conditions and used the results to develop and test a general degradation model for DSCs. Usually, the existing predictive models for emerging PVs require a significant loss of performance before the predictions become accurate—limiting the added value from the predictions. This is due to the

A. Poskela, H. Palonen, K. Miettunen
Department of Mechanical and Materials Engineering
Faculty of Technology
University of Turku
Turku FI-20014, Finland
E-mail: aapo.poskela@utu.fi

A. Poskela, P. D. Lund
Department of Applied Physics
School of Science
Aalto University
Espoo FI-00076, Finland

A. Tiihonen, K. Miettunen
Department of Bioproducts and Biosystems
School of Chemical Engineering
Aalto University
Espoo FI-00076, Finland

A. Tiihonen
Department of Mechanical Engineering
Massachusetts Institute of Technology
Cambridge, MA 02139, USA

The ORCID identification number(s) for the author(s) of this article can be found under https://doi.org/10.1002/solr.202101004.

DOI: 10.1002/solr.202101004

challenging domain for the predictions. It is typical for an emerging PV to experience nonlinear and rather complex degradation behavior, which may involve long initial periods of full stability or even increases in efficiency before the onset of degradation. In some cases, the losses may behave exponentially, which is challenging to predict since small changes in the fit parameters may lead to large differences in the time point of interest far away.

Here, we focus onDSCs, which are low cost and can be prepared from nontoxic materials.[22,23] Specifically, we demonstrate that the optical analysis of the changes in the DSC electrolyte color occurring early on in an aging test, can be used as a valid proxy to the loss of charge carriers, and therefore used to predict the loss of performance of the solar cells. By tracking the loss rate of charge carriers directly, we can predict performance loss before it is visible in the more traditionally used current–voltage (*I*–*V*) measurement data. The main advantages of our method are: i) short, simple, and high-throughput compliant in situ measurements, and ii) good predictive accuracies achieved already during the early stages of aging tests. We also investigate the potential for using electrochemical impedance spectroscopy data for predictive modeling, as the loss of charge carriers can also be tracked using impedance spectroscopy. These results provide insight into the type of model parameters that should be chosen to produce the most relevant predictive models for PVs.

2. Experimental Section

2.1. Sample Preparation

The DSC samples had a standard sandwich structure, where the active components of the cells were sealed between two fluorine-doped tin oxide (FTO) glass substrates. The cell structure prioritized long lifetime and easy visual analysis rather than high PV performance. The glasses were attached by melting a 40 μm thick Surlyn 1702 ionomer resin film (DuPont) frame between the glass substrates. The glass substrates were cleaned with mild dishwashing detergent, then sonicated in Hellmanex® III (Hellma Analytics), followed by ethanol and finally in acetone. The substrates were UV treated with a UV/Ozone ProCleaner™ (Bioforce Nanosciences) before they were used in the sample assembly.

The photoelectrode of the DSCs was nanostructured TiO_2, sensitized with Z907 dye. Before the photoelectrode was made, a compact TiO_2 layer was deposited on the substrate by immersing it in deionized water with 1 wt% of titanium(IV) chloride tetrahydrofuran complex for 30 min at 70 °C. The TiO_2 film was prepared by screen printing (AT-60PD, ATMA) two layers of smaller TiO_2 particles (DSL 18NR-T, Dyesol) and one layer of light scattering particles (DSL 18NR-AO, Dyesol). The photoelectrode was sintered for 30 min at 450 °C. Another compact TiO_2 layer was added to the photoelectrodes using the same methods as previously described, followed by another sintering. The photoelectrodes were finalized by immersing them in a 0.3 mM Z907 (Dyesol) 1:1 acetonitrile (ACN) and tert-butylalcohol (tBA) solution for ≈16 h.

The counter electrode was coated with a Pt catalyst using 4 μl of 10 mM H_2PtCl_6 in 2-propanol. The solution was applied to the surface of the substrate using a micropipette. After the solvent had evaporated, the counter electrodes were heated for 20 min in an oven set to 390 °C.

Once the electrodes had been attached to each other by melting a frame of Surlyn™ ionomer resin film, the DSC was filled with a liquid electrolyte through holes in the counter electrode substrate. The electrolyte used in this study had I^-/I_3^- redox couple and it contained 0.05 M I_2, 0.5 M 1-methylbenzimidazole (NMBI), 0.5 M 1-propyl-3-methylimidazolium iodide (PMII), and 0.1 M guanidium thiocyanate (GuSCN) in 3-methoxypropionitrile.

The holes in the substrate were closed by attaching a microscope glass to the substrate by melting a piece of Surlyn™ ionomer resin between them, thus sealing the solar cells from ambient conditions. The electric contacts for the DSCs were formed by attaching copper tapes to both of the electrodes. The contact was improved by painting the contacts between the electrodes and the tapes with silver paint (SCP, Electrolube). Finally, the mechanical robustness and the sealing of the cells were secured by coating the interface between the electrodes with epoxy glue. The finished cells were stabilized under halogen lamps and UV filters for 10 h before the measurements.

2.2. Aging and Measurements

The DSCs were aged in two different solar simulators. One simulator illuminated the cells at ambient temperature and humidity with white CREE Edge HO240 LEDs (light-emitting diodes). The temperature of the cells under LED illumination was stable at 40 ± 1 °C. The other aging simulator was a Suntest XLS+ (Atlas) with a xenon arc lamp (NXE 1700, Atlas), cooling fans, and ambient humidity. At full cooling, the temperature of these cells remained at 55 ± 2 °C. Unlike the white LEDs, the xenon arc lamp emitted light at UV wavelengths that are a strong degradation factor for DSCs. Therefore, a UV filter (Asmetronic SFC-10 UV filter[24]) was used to limit the harmful effects of UV illumination on the DSCs. The UV filter was on a separate holder on top of the samples, thus the cells were photographed without the filter. The degradation related to different kinds of aging spectra and the effects of UV filtering is discussed in our previous publication,[24] while here the focus is solely on predicting the degradation pattern. The aging setup was set to automatically measure the cells during aging. BioLogic SP-150 potentiostat and an Agilent 34 980 A Multifunction Switch/Measure Unit measured the *I*–*V* curves and the electrochemical impedance spectra (EIS) of each of the cells. The scan rate of the *I*–*V* measurement was 5 mV s^{-1} and the impedance measurement voltage frequency ranged from 0.1 Hz to 100 kHz with an amplitude of 10 mV. Between the measurements, the cell was connected to an open circuit.[25] The EIS results were analyzed using Zview2 (Scribner Associates, Inc.).

Photograph analysis has been used earlier in the literature to investigate both the electrolyte[26] and the dye[27,28] for DSCs. The automated measurements were supported by weekly photographing of the cells. All of the samples were measured in a separate system with its own light source to prevent differences in the illumination to impact the measurement. The DSCs were disconnected from the automated measurement system and

moved to a specifically designed photographing chamber. The samples in the chamber were illuminated with white LEDs, while all ambient light was blocked to prevent it from affecting the photographs. The digital photographs were taken with an Olympus E-620 camera. The camera was set to RAW image format with AdobeRGB colors, aperture f/8.0, sensitivity ISO100, 1/20 s exposure, and manual focus. The accuracy of prediction was strongly dependent on the quality of the digital photographs and their analysis; therefore, it is important to ensure that the lighting conditions, methods, and equipment used to take the images are consistent in each measurement. To further ensure that the photographs taken on different weeks were comparable, a color profile was generated using a color checker passport (X-Rite) and then applied to the images with Adobe Lightroom.[26] A MATLAB script was used to extract the average Red, Green and Blue (RGB) values from an area of the DSC electrolyte not covered by the photoelectrode. The blue value (B) was then converted to the yellow value (Y) of the cyan, magenta, yellow (CMY) color space with a simple formula $Y = 255 - B$. The CMY color space is the complement of the RGB color space.[29] The CMY color space was used since we track bleaching of yellow color, making it more intuitive to follow changes in Y values.

In addition to the repeated automated measurements during aging, the more accurate 1 sun I–V curves of the DSCs were measured under a standard AM1.5G spectrum at the start and the end of the aging test. The AM1.5G illumination was simulated with a Peccell PEC-01 solar simulator and the curves were recorded with a Keithley 2420 3 A Sourcemeter.

2.3. Color Analysis Predictive Model Description

The goal of the color analysis predictive model was to predict the development of the short-circuit current (I_{SC}) for a DSC as the cell degrades. This is achieved by considering the limiting current (I_{lim}) of the DSC, which was the highest current that the DSC is capable of generating. DSC operation relied on redox reactions to regenerate the photoelectrode after its photoexcited electrons were injected into an external circuit to generate current. The redox charge carriers were diffused from the counter electrode to the photoelectrode through an electrolyte within the cell, but the regeneration rate is limited by diffusion. Thus, when increasing the current drawn from a DSC, eventually the photoelectrode cannot be regenerated any faster since its surface is depleted of charge carriers[30,31] due to the limited diffusion rate of the replacement charge carriers through the electrolyte. The current at which diffusion restrictions limit a further increase in the current was the limiting current I_{lim}, which can be expressed as[31]

$$I_{lim} = \frac{4FD_{I_3^-}c_{I_3^-}}{d} \quad (1)$$

where F is the Faraday constant, d is the distance between the electrodes, and $D_{I_3^-}$ and $c_{I_3^-}$ are the diffusion coefficient and concentration of tri-iodide redox species, respectively. It should be noted that the diffusion coefficient and concentration in Equation (1) were for tri-iodide (I_3^-). While the redox reactions were between a pair of charge carriers, tri-iodide, and iodide (I^-), the rate of diffusion of tri-iodide is typically the limiting factor. The diffusion coefficient of both charge carriers was similar, but the concentration ($c_{I_3^-}$) of tri-iodide was typically much lower than that of iodide. Increasing the concentration of tri-iodide would increase I_{lim}, but that in turn would amplify recombination and optical losses at the photoelectrode.[31]

The diffusion coefficient $D_{I_3^-}$ can be calculated from Equation (1) for a fresh DSC sample when $c_{I_3^-}$ is known and I_{lim} is measured. I_{lim} can be measured by either exposing the cell to high-intensity illumination, or from the reverse bias region in an I–V curve measured in the dark.[32,33] These measurements should be used with care, since exposure to high intensities may heat the cells and high reverse bias can affect cell performance. Using values measured by Mastroianni et al.[32] for a DSC with a I_3^-/I^- redox couple, the diffusion coefficient $D_{I_3^-}$ was between 6.8×10^{-6} and 7.5×10^{-6} cm^2 s^{-1} (for $c_{I_3^-} = 0.050$ and 0.025 mol dm^{-3}, respectively) at room temperature. As the diffusion coefficient was dependent on the concentration of the diffusing species, and the concentration of I_3^- decreased during aging, the range above was used as minimum and maximum degradation rate cases for the predictive model. It was verified in an earlier study[26] that the blue pixel value relating to tri-iodide concentration changes linearly below 0.1 mol dm^{-3}.

Once the values of the parameters are solved for the DSC in its initial state, the changes that occur as the cell degrades must be estimated. The main degradation pathway in a DSC is the loss of charge carriers in the electrolyte.[24,32] As can be seen from Equation (1), a decrease in the concentration of I_3^- will also linearly decrease the limiting current I_{lim}. Therefore, by measuring the rate of decrease for $c_{I_3^-}$, the rate of decrease for I_{lim} can be calculated and how it will eventually limit the output current of the DSC even in typical operating conditions.

The tri-iodide concentration $c_{I_3^-}$ of a DSC can be measured in situ by tracking the color of its electrolyte. I_3^- has a strong yellow color, and as it degraded to other compounds the color fades. This is called bleaching of the electrolyte.[26,32] In other words, tri-iodide absorbed blue light effectively, causing light reflected from the electrolyte to appear yellow. A decrease in tri-iodide concentration decreased the absorption of blue light. By systematically photographing the degrading DSCs, the rate at which their electrolyte bleaches was determined, which in turn can be converted to the rate of the I_3^- concentration loss. In a previous study,[32] this rate was found to be between 0.65 and 0.91 mM/Y, where Y is the yellow value in a CMY color space. The decrease in concentration can be converted to the lowering of the limiting current with Equation (1), giving a range of 0.29 . . . 0.40 mA/Y. This rate was used to determine the rate of I_{lim} degradation by measuring the color change in the electrolyte during the first days of aging, then linearly extrapolating it to predict how the cell current will decrease. Note that the values presented here for the relation between $c_{I_3^-}$ and yellow color were defined for our sandwich cell configuration and would require adjustment to different cell configurations (**Table 1**).

Table 1. The values used by the color analysis predictive model in Equation (1). The source of each value is shown in "Details".

Parameter	Symbol	Value	Details
Faraday constant	F	96 485.33 A s mol^{-1}	Physical constant
Distance between the electrodes	d	40 µm	The thickness of the spacer used between the glass electrodes in cell preparation.
Diffusion coefficient of I_3^- charge carriers	$D_{I_3^-}$	6.8×10^{-6} ... 7.5×10^{-6} cm^2 s^{-1}	Range calculated from the results of previous studies using Equation (1).[26,32]
I_3^- concentration	$c_{I_3^-}$	0.050 mol L^{-1} (Initially)	Decreases as the aging progresses. Decrease is detected as bleaching of the electrolyte 0.654...0.909 mM Y^{-1}. The initial amount was estimated from the preparation of the electrolyte.[31]

To summarize, the limiting current I_{lim} of DSC samples were measured after they were assembled, then its development was predicted by measuring and extrapolating the loss of charge carriers during the early aging test. The loss of charge carriers was estimated by analyzing the bleaching of the electrolyte from digital photographs of the DSC samples.

2.4. Diffusion Resistance Model Description

There is an alternative approach to predict the loss of charge carriers in DSC electrolyte. This method does not rely on photographing of the cells, but instead uses impedance of different DSC components measured throughout the aging test with EIS. The diffusion resistance R_{D} of DSC electrolyte is dependent on the concentration of tri-iodide charge carriers as

$$R_{\text{D}} = \frac{k_B T \delta}{n^2 q^2 D_{I_3^-} c_{I_3^-}} \tag{2}$$

where k_B is the Boltzmann constant, T is the temperature, δ is half of the electrolyte layer thickness, n is the number of electrons transferred in the overall redox reaction, and q is the elementary charge.[31] By combining this with Equation (1), it was shown that the limiting current depends on the diffusion resistance as

$$I_{\text{lim}} = \frac{2Fk_B T}{3n^2 q^2 R_D} \tag{3}$$

Once the concentration has decreased enough that the charge carrier concentration limited the performance $I_{\text{SC}} = I_{\text{lim}}$. It was established that I_{lim} is inversely proportional to R_{D}, which can be measured with EIS. If the change in R_{D} from early measurements can be extrapolated, then the decrease in cell current can be predicted similar to the color analysis predictive model described earlier. The difference between the two methods is the recurring measurement technique required: periodic photography or EIS measurements. Equation (2) suggests that R_{D} increases inversely when it is assumed that the tri-iodide concentration decreases linearly.[26] Therefore, a function in the following form is used.

$$R_{\text{D}} = -a \cdot (t - b)^{-1} + c \tag{4}$$

where a, b, and c are coefficients to be determined by fitting (a, $b \geq 0$) and t is the independent variable time. Additionally, the R_{D} time series was fitted to a single exponential function for comparison.

$$R_{\text{D}} = a' e^{b' x} \tag{5}$$

where coefficients a' and b' are positive fitting parameters.

3. Results and Discussion

3.1. Colour Analysis Predictive Model Results

The initial PV performance of the assembled DSCs is presented in **Table 2**. The components of the cells were chosen with stability testing as the main purpose. The area of the cell which is filled with electrolytes is wider than the actual active area of the cell. This cell configuration introduces losses in the DSC power conversion efficiency but facilitates determining the color of the electrolyte from photographs. **Figure 1** shows example photographs taken in the first 1000 h of the aging for a single sample. The images also indicate the area from which the color is analyzed and the average color from that area. Note that the analyzed area was to the side of the photoelectrode, where the electrolyte is exposed without the dyed TiO_2 layer. Such an area is not always available in some cell configurations. An alternative method would be to take the images from the backside of the DSCs, but the accuracy of this method depends on the color of the dyed TiO_2 and its consistency across different samples.

Figure 2 illustrates how each of the RGB colors develop during the aging test for all the cells. It is important to note that the red and green components remain stable for the whole duration, while only the blue value increases. The increase of the blue color means that yellow—the complementary color for blue—is decreasing, due to the electrolyte bleaching as described in the previous section. The yellow component of the electrolyte color was used to predict the evolution of the limiting current with Equation (1). **Figure 3** displays the predicted average lifetimes and their deviations from two different points in aging: the first is made after 336 h of aging with three color

Table 2. Initial performance indicators of DSCs used for the color analysis predictive model. The values are averages and standard deviation calculated from 29 samples.

Short-circuit current density [J_{SC}]	10.5 ± 0.4 mA cm^{-2}
Open circuit voltage (V_{OC})	787 ± 8 mV
Fill Factor (FF)	63 ± 2
Efficiency (η)	5.2 ± 0.2%

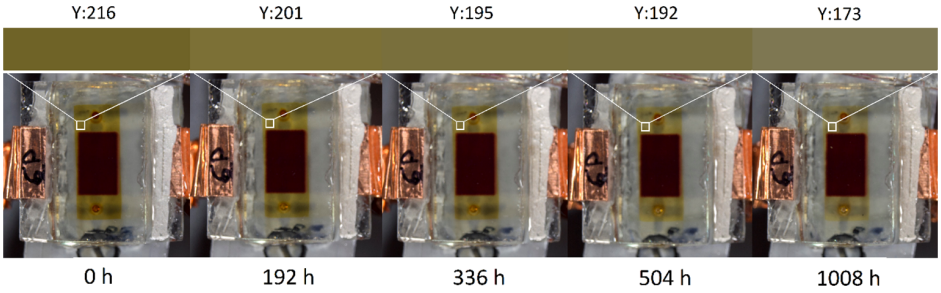

Figure 1. Digital photographs of an example cell at five points during the first 1008 h of aging. A white square in the images shows the area used in the color analysis. The RGB values were calculated as the average of all the pixels in this area. Above the images is a color bar showing the measured color, and the yellow (Y) value calculated from the blue (B) value as $Y = 255 - B$.

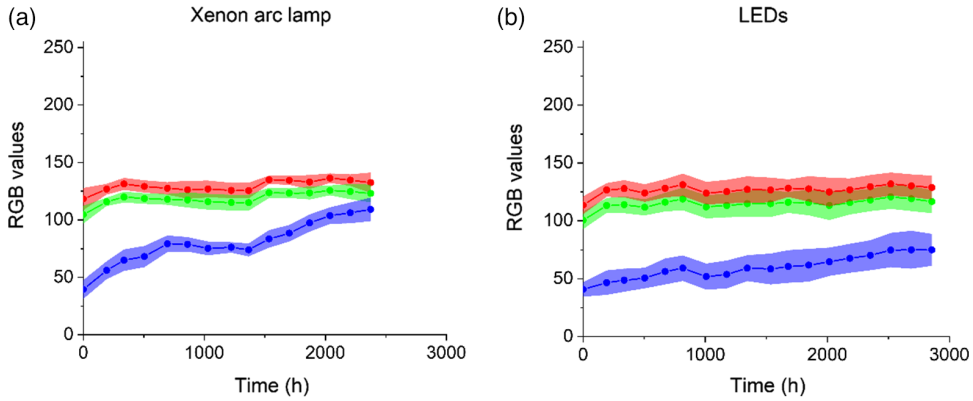

Figure 2. The development of RGB values during aging for: a) DSCs aged under Xenon arc lamps and b) DSCs aged under LEDs. The colors of the lines represent each of the RGB colors. The colored region is the standard deviation of the samples. Both groups of cells had 9 individual samples.

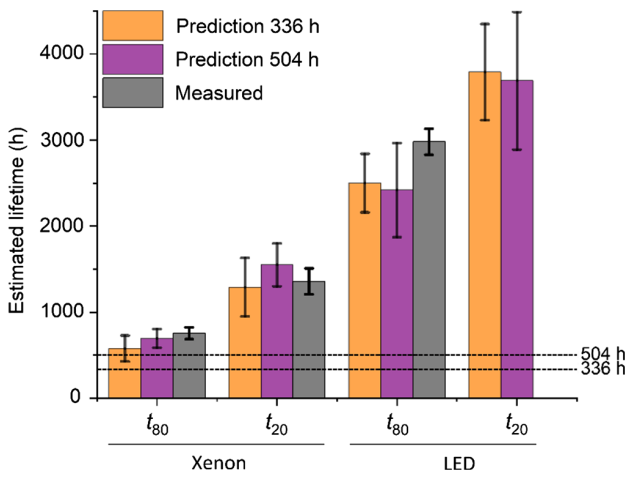

Figure 3. Predicted lifetime indicators for DSC samples aged under Xenon arc lamps or LEDs. t_{80} and t_{20} are the times when cell efficiency has decreased to 80% and 20% of the peak value. The color analysis predictive model was run twice: 336 and 504 h after the start of the aging. Also, the measured values are shown. Cells aged under LEDs did not reach the t_{20} during the aging.

measurements and the second is made after 504 h with four data points. t_{80} and t_{20} are the times when the cells have reached 80% and 20% of their initial efficiency, respectively. The accuracy of the prediction is excellent for cells aged under xenon lamps, with both t_{80} and t_{20} lifetimes successfully within the prediction intervals. The prediction accuracy was lower for LED-illuminated DSCs. The lower accuracy is caused by the significantly longer lifetime for LED-illuminated samples: the bleaching of the electrolyte is slower due to the lack of UV light and is harder to accurately determine during early aging. The measured t_{80} was about 500 h longer than the 2500 h the color analysis predictive model predicted. The DSC samples did not reach t_{20} during the aging test since it was terminated after 3000 h, while the prediction was closer to 4000 h.

An example of a prediction for the DSCs degraded under xenon arc lamp illumination is shown in **Figure 4**a,b. The earlier prediction made after 336 h of aging already correctly predicted the rate of degradation and estimated the degradation of the current mostly within the error margins of the model (Figure 4a). The prediction made at 504 h improved the accuracy even further with a remarkable match with the predicted current (Figure 4b). In the case of aging under LED lights, the measured current is within the range of the prediction made after 504 h (Figure 4c). The 336-hour prediction, however, underestimates the lifetime of the DSCs (Figure 4d). This is likely because the solar cells clearly have longer lifetimes under LED illumination, i.e., slower bleaching, and the number of sample photographing sessions is insufficient to accurately estimate the

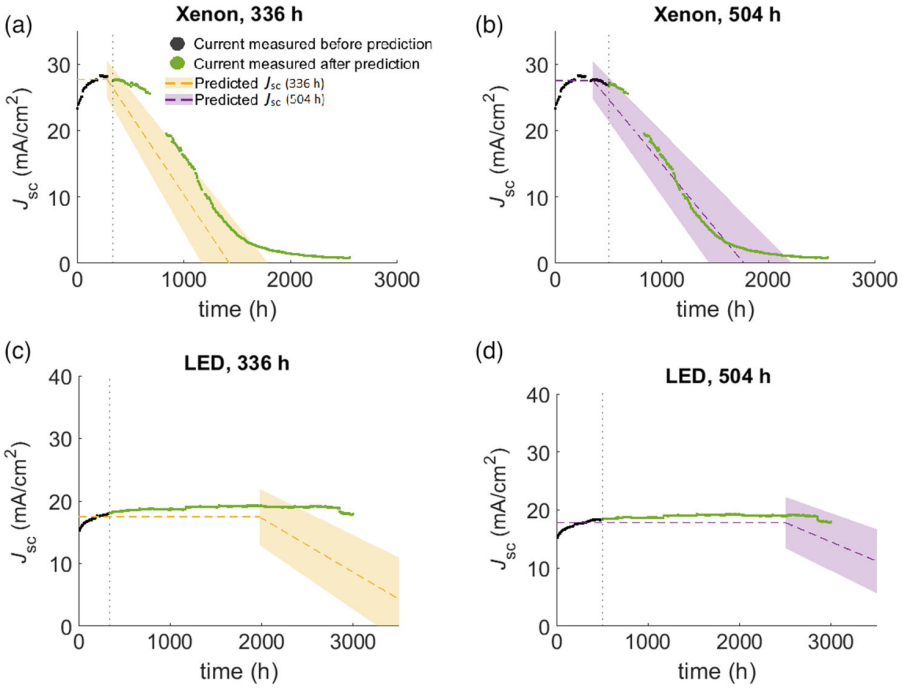

Figure 4. Predicted short-circuit current calculated from electrolyte color changes compared to measured current when DSCs were aged under: a,b) xenon arc lamps and c,d) LEDs. Colored area for the predicted short-circuit current shows the uncertainty that takes into account the inaccuracies in the diffusion coefficient and in yellow color to charge carrier conversion. The prediction was made: a,c) after 336 h of aging, and b,d) after 504 hours of aging, indicated with a dashed line. The initial predicted current value is calculated from the average measured current between 100 h and the prediction time, which is the only fitting parameter from measured current values used in the prediction. Gap in the current data for DSCs aged under xenon lamps is caused by a data collection error.

slope of the color bleaching for this slow degradation. This demonstrates that slower degradation requires a longer data collection time, or more frequent photographing measurements.

As an alternative predictive method, we tested predicting the decrease of the limiting current by extrapolating the increase of diffusion resistance R_D caused by the loss of charge carriers. The measured values of all EIS parameters for these DSCs are visible in an earlier publication.[24] Time-inverse (Equation (4)) and single exponential (Equation (5)) models were fitted to R_D values measured during the first 504 h of the aging test. The results shown in **Figure 5** illustrate that the extrapolative models are unable to correctly predict the slope of the R_D increase that happens long after the time of prediction. The unpredictability is illustrated in the time-inverse function fit giving wildly different results when fitted to the data after 400 or 500 h of aging. The exponential function—that has no physics-based justification—has better accuracy but fails to reproduce the rapid increase in R_D once the concentration of charge carriers is low. The inaccuracy of the prediction arises from the nonlinearity of the extrapolated function, since it is challenging to find the correct fit without information about the location of the curve in a time-inverse function. The same observation holds for the exponential function. Our prediction through image analysis overcomes this issue, since it relies on the color of the electrolyte which is linearly related to the limiting current of a DSC, and

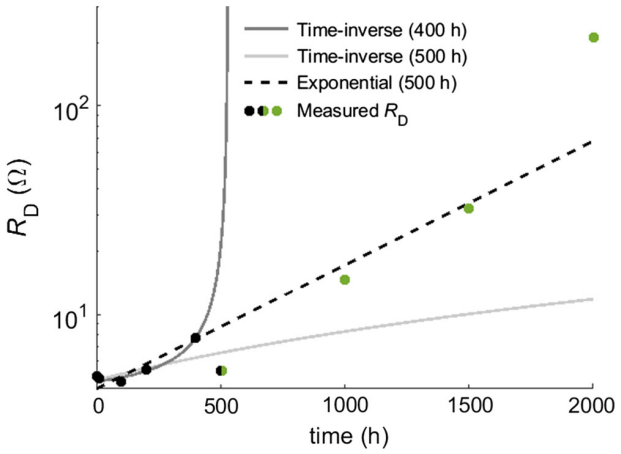

Figure 5. A general time-inverse Equation (4) and a single exponential function fitted to the R_D of an example cell under xenon arc lamp. The time-inverse function is fitted after 400 h and 500 h after the start of the aging process and the single exponential 500 h after the start. The single exponential model is included as a comparison to illustrate how well a model without physics-based reasoning performs. Measurement points are colored black until 400 h and green beyond 500 h to illustrate the prediction. The data point that was used in the 500 h-predictions is half-colored. The prediction moments differ from the color analysis method since the EIS data was analyzed at exactly every 100 h.

changes in it are clearly visible early in the aging. This example of the EIS-based models demonstrates that even when the models link to the same underlying degradation mechanism, the loss of charge carriers in the electrolyte, the exact choice of the physics-based parameters of the model, here either R_D or electrolyte color, bears importance for the accuracy of the predictions. Similar considerations on the stability of the chosen physics-based parameters also hold true for other solar cell types.

The most important aspects to consider when utilizing the predictive color analysis model are: 1) the accuracy of the initial values for $D_{I_3^-}$, 2) the link between the loss of charge carriers and electrolyte bleaching, and 3) the assumed role of electrolyte bleaching in the degradation. The model relies on the assumption that electrolyte bleaching is the most severe degradation factor, which holds for most DSCs apart from early-phase experimental photoelectrode materials. $D_{I_3^-}$ and how the loss of charge carriers connects to electrolyte bleaching depend on the specifics of the cell types under investigation. They need to be determined before the color analysis method can be used to predict lifetime. The accuracy and repeatability of the photographing process is a key practical consideration for the success of the prediction. Turning ordinary photographs to quantitative and reproducible measurement data requires in practice both stable illumination conditions and color calibration to transform the observed colors to a stable reference color space.

It is worth mentioning that while this study uses iodide/tri-iodide redox electrolyte, the method described here should work on any type of electrolyte that demonstrates color change as it degrades. Our previous study[34] revealed similar effects in a cobalt complex electrolyte, but the color change was smaller in magnitude. Smaller changes require high accuracy for the image analysis to give reliable results.

3.2. Comparison to Other Models

We applied the extrapolation model introduced by Rizzo et al.[20] to compare its performance to the color analysis predictive model presented here. The extrapolation model was implemented with a MATLAB script using Hampel filters for data smoothing and outlier removal. The extrapolation fit was attempted using three different functions: a linear polynomial, single exponential, and double exponential. The predictions with both models were made 504 h after the beginning of aging (**Figure 6**). The double exponential version clearly performs the best among the extrapolative models. The polynomial and single exponential versions are strongly affected by the initial increase in the short-circuit current, which diverts them to increase infinitely. Even if the initial current stabilization is removed from the data, the extrapolative models are unable to predict the degradation without moving the moment of prediction to later, so that the shape and the rate of degradation are clearer. The model based on the color changes of the DSC electrolyte performed more accurately in both cases than the more general models relying on extrapolation. A major advantage of the color analysis predictive model is its ability to use the physical properties of the DSC to capture changes in the cell before they are apparent in the measured performance indicators such as the current. This is especially valuable when studying DSCs, which display nonlinear degradation behavior: initially, the current of the cells appears to remain stable, until it suddenly starts to rapidly decrease. This happens because the limiting current starts to limit the short-circuit current extracted from the DSC under standard illumination conditions. A model that relies on extrapolation will fail to predict this nonlinear behavior if the prediction is made before the rapid decrease of performance begins. Making a prediction after the rapid loss of performance has begun is not as useful as the early predictions, since the DSCs will likely completely degrade relatively soon after.

4. Conclusions

In this contribution, we present the first predictive model for DSCs—an emerging PV technology—that is based on in situ measurements at the early stage of stability testing, when the PV performance remains unaffected by degradation. Our predictive model was based on color changes in the electrolyte of a DSC, serving as an indicator of the loss of charge carriers in the electrolyte. Lifetime predictions with our model after 504 h of aging were correct within the error margins for all DSCs that degraded in the first 2500 h of aging. The method of predicting lifetime from photographs is a frugal, low-cost, and high-throughput compatible approach compared to more complex measurements such as EIS-based analysis, which we also showed to be less accurate.

While our color analysis predictive model was able to capture the degradation accurately, different extrapolative methods were

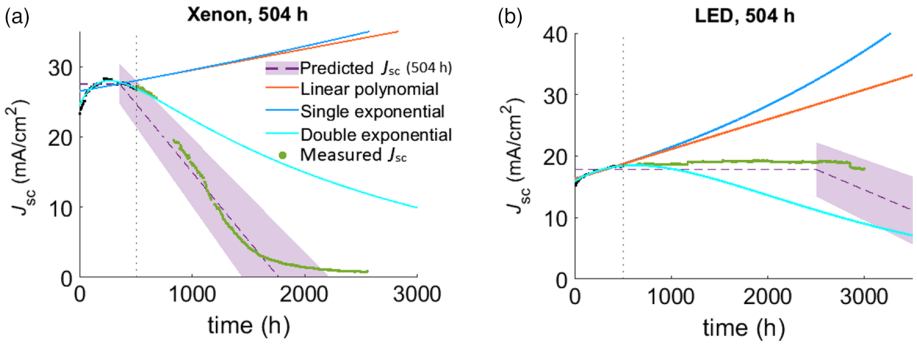

Figure 6. Predictions made with different extrapolation fits. All the predictions were made after 504 h of aging. a) Demonstrates a DSC aged under xenon arc lamp and b) a DSC under LEDs. Our colour analysis prediction is signified by the purple range, with the average marked using a dashed line.

unable to do so at such an early stage of testing. The key to the success of our model lies in the linear behavior of the electrolyte color. The extrapolative methods depend on diffusion resistance or current, both of which behave nonlinearly. Capturing the nonlinearity is challenging from early measurement data. Adopting predictive methods more widely for emerging solar cell stability research could accelerate efforts to find material combinations that would extend PV lifetime. In doing so, these promising PV technologies could be commercialized. Analyzing color changes to predict performance degradation could also have direct applications for perovskite solar cells, since perovskite degradation induces a visible color change. Photographing could also be used to study spatial differences of the tri-iodide concentration in the electrolyte. Such a study could reveal concentration gradients caused by reactions with the photoelectrode and the counter electrode, or undesirable reactions at the sealant interface.

Acknowledgements

A.P., A.T., and K.M. thank Academy of Finland, project BioEST (project numbers 318557, 336577, 320100, 336441).

Conflict of Interest

The authors declare no conflict of interest.

Data Availability Statement

The data that support the findings of this study are available from the corresponding author upon reasonable request.

Keywords

color analysis, degradation, dye solar cells, lifetime prediction, stability

Received: November 29, 2021
Revised: January 19, 2022
Published online: February 11, 2022

[1] M. I. Asghar, K. Miettunen, J. Halme, P. Vahermaa, M. Toivola, K. Aitola, P. Lund, *Energy Environ. Sci.* **2010**, *3*, 418.
[2] S. A. Gevorgyan, I. M. Heckler, E. Bundgaard, M. Corazza, M. Hösel, R. R. Søndergaard, G. A. Dos Reis Benatto, M. Jørgensen, F. C. Krebs, *J. Phys. D. Appl. Phys.* **2017**, *50*, 103001.
[3] M. I. Asghar, J. Zhang, H. Wang, P. D. Lund, *Renew. Sustain. Energy Rev.* **2017**, *77*, 131.
[4] C. H. M. Chuang, P. R. Brown, V. Bulović, M. G. Bawendi, *Nat. Mater.* **2014**, *13*, 796.
[5] G. TamizhMani, J. Kuitche, *Accelerated Lifetime Testing of Photovoltaic Modules, Solar America Board for Codes and Standards*, July **2013**, https://www.solarabcs.org. (accessed: October 2021).
[6] J. Wohlgemuth, D. Cunningham, in *23rd European Photovolt. Sol. Energy Conf. Exhib.*, **2008**, p. 2663.
[7] B. Mitchell, D. Chung, Q. He, H. Zhang, Z. Xiong, P. P. Altermatt, P. Geelan-Small, T. Trupke, *IEEE J. Photovoltaics* **2017**, *7*, 1619.
[8] H. Wagner, M. Müller, G. Fischer, P. P. Altermatt, *J. Appl. Phys.* **2013**, *114*, 054501.
[9] I. Kaaya, S. Lindig, K. A. Weiss, A. Virtuani, M. Sidrach de Cardona Ortin, D. Moser, *Prog. Photovoltaics Res. Appl.* **2020**, *28*, 979.
[10] P. Hacke, R. Smith, K. Terwilliger, S. Glick, D. Jordan, S. Johnston, M. Kempe, S. Kurtz, in *2012 IEEE 38th Photovolt. Spec. Conf. PART 2*, IEEE, USA **2014**, p. 1.
[11] K. Takahisa, T. Kojima, K. Nakamura, T. Koyanagi, T. Yanagisawa, *Sol. Energy Mater. Sol. Cells* **1997**, *49*, 179.
[12] R. Laronde, A. Charki, D. Bigaud, *J. Sol. Energy Eng. Trans. ASME* **2013**, *135*, 1.
[13] M. Vázquez, I. Rey-Stolle, *Prog. Photovoltaics Res. Appl.* **2008**, *16*, 419.
[14] B. Nehme, N. K. M'Sirdi, T. Akiki, A. Naamane, *Energy Procedia* **2014**, *62*, 565.
[15] A. Charki, *J. Photonics Energy* **2013**, *3*, 033099.
[16] B. Ray, M. A. Alam, *Appl. Phys. Lett.* **2011**, *99*, 1.
[17] M. A. Arshad, A. K. Maaroufi, *J. Power Sources* **2018**, *391*, 134.
[18] J. Kim, N. Park, J. S. Yun, S. Huang, M. A. Green, A. W. Y. Ho-Baillie, *Sol. Energy Mater. Sol. Cells* **2017**, *162*, 41.
[19] J. P. Bastos, G. Uytterhoeven, W. Qiu, U. W. Paetzold, D. Cheyns, S. Surana, J. Rivas, M. Jaysankar, W. Song, T. Aernouts, J. Poortmans, R. Gehlhaar, *ACS Appl. Mater. Interfaces* **2019**, *11*, 16517.
[20] A. Rizzo, A. Cester, M. V. Madsen, F. C. Krebs, S. A. Gevorgyan, *Small Methods* **2018**, *2*, 1.
[21] D. A. Chalkias, D. D. Loizos, G. C. Papanicolaou, *Sol. Energy* **2020**, *207*, 841.
[22] A. B. Muñoz-García, I. Benesperi, G. Boschloo, J. J. Concepcion, J. H. Delcamp, E. A. Gibson, G. J. Meyer, M. Pavone, H. Pettersson, A. Hagfeldt, M. Freitag, *Chem. Soc. Rev.* **2021**, https://doi.org/10.1039/d0cs01336f.
[23] A. Hinsch, W. Veurman, H. Brandt, K. Flarup Jensen, S. Mastroianni, *ChemPhysChem* **2014**, *15*, 1076.
[24] A. Poskela, K. Miettunen, A. Tiihonen, P. D. Lund, *Energy Sci. Eng.* **2021**, *9*, 19.
[25] A. Poskela, K. Miettunen, A. Tiihonen, P. D. Lund, *Electrochim. Acta* **2018**, *275*, 59.
[26] M. I. Asghar, K. Miettunen, S. Mastroianni, J. Halme, H. Vahlman, P. Lund, *Sol. Energy* **2012**, *86*, 331.
[27] T. Watson, P. Holliman, D. Worsley, *J. Mater. Chem.* **2011**, *21*, 4321.
[28] P. J. Holliman, M. L. Davies, A. Connell, B. V. Velasco, T. M. Watson, *Chem. Commun.* **2010**, *46*, 7256.
[29] A. Kriegl, *The CMY Color Model*, **2003**, https://www.mat.univie.ac.at/~kriegl/Skripten/CG/node13.html. (accessed: November 2021).
[30] L. Bay, K. West, B. Winther-Jensen, T. Jacobsen, *Sol. Energy Mater. Sol. Cells* **2006**, *90*, 341.
[31] J. Halme, P. Vahermaa, K. Miettunen, P. Lund, *Adv. Mater.* **2010**, *22*, E210.
[32] S. Mastroianni, I. Asghar, K. Miettunen, J. Halme, A. Lanuti, T. M. Brown, P. Lund, *Phys. Chem. Chem. Phys.* **2014**, *16*, 6092.
[33] K. J. Seo, K. A. Bialecka, M. S. Kang, A. Hinsch, S. H. Moon, *J. Power Sources* **2015**, *275*, 675.
[34] K. Miettunen, A. Poskela, A. Tiihonen, S. Rendon, K. Axenov, L. Kronberg, R. Leino, P. D. Lund, *Nano Energy Syst.* **2017**, *1*, 29.